Electrostatic attraction of weak monoacid anions increases probability for protonation and passage through aquaporins

Received for publication, February 21, 2017, and in revised form, March 28, 2017 Published, Papers in Press, March 30, 2017, DOI 10.1074/jbc.M117.782516

Monja Rothert, Deike Rönfeldt[1], and Eric Beitz[2]

From the Department of Pharmaceutical and Medicinal Chemistry, Christian-Albrechts-University of Kiel, 24118 Kiel, Germany

Edited by Thomas Söllner

A positive electrostatic field emanating from the center of the aquaporin (AQP) water and solute channel is responsible for the repulsion of cations. At the same time, however, a positive field will attract anions. In this regard, L-lactate/lactic acid permeability has been shown for various isoforms of the otherwise highly water and neutral substrate selective AQP family. The structural requirements rendering certain AQPs permeable for weak monoacids and the mechanism of conduction have remained unclear. Here, we show by profiling pH-dependent substrate permeability, measurements of media alkalization, and proton decoupling that AQP9 acts as a channel for the protonated, neutral monocarboxylic acid species. Intriguingly, the obtained permeability rates indicate an up to 10 times higher probability of passage via AQP9 than given by the fraction of the protonated acid substrate at a certain pH. We generated AQP9 point mutants showing that this effect is independent from properties of the channel interior but caused by the protein surface electrostatics. Monocarboxylic acid-conducting AQPs thus employ a mechanism similar to the family of formate-nitrite transporters for weak monoacids. On a more general basis, our data illustrate semiquantitatively the contribution of surface electrostatics to the interaction of charged molecule substrates or ligands with target proteins, such as channels, transporters, enzymes, or receptors.

Tetrameric cellular water and solute channels of the aquaporin family (AQP)[3] are highly selective for water or additionally permit the passage of small, neutral solutes, such as glycerol and urea (1, 2). The respective subfamilies are termed "orthodox AQPs" and "aquaglyceroporins." Generally, AQPs are characterized by the strict exclusion of positively charged ions including protons (3–8). The cations are repelled by a positive electrostatic field emanating from the central region of the conduction path of the individual AQP protomer, *i.e.* the Asn-Pro-Ala (NPA) constriction (3, 6). A second, even narrower constriction site positioned toward the extracellular side of the AQP contributes to the exclusion of cations because of its composition of a conserved, positively charged arginine residue in an aromatic environment (ar/R) (4, 5, 7, 8) and further acts as a substrate selectivity filter by size (4, 9). However, an electrostatic field that repels cations must, at the same time, attract anions. In fact, there are reports stating anion permeability of selected AQPs.

Mammalian AQP6 is the most prominent example exhibiting true anion channel properties with conductance, *e.g.* for NO_3^- and Cl^- (10, 11). As anions of the strong nitric and hydrochloric acids, these substrates are fully dissociated and thus negatively charged throughout the whole physiological pH range. Anion conductance of AQP6 is explained by a structural peculiarity, *i.e.* an asparagine residue instead of an otherwise perfectly conserved glycine at a helix crossing point, which allows for slippery helix movements that widen the channel permitting passage of partially hydrated anions (12). The situation regarding the protonation state of weak acid substrates, such as organic monocarboxylates, is more complex (13). There are several reports on monocarboxylate permeability of AQPs, mainly for lactate/lactic acid, *e.g.* NIP1;2 (nodulin-26-like intrinsic protein 1;2) of *Arabidopsis thaliana* (14), the *Schistosoma mansoni* AQP (15), the glycerol facilitator GlpF of *Lactobacillus plantarum* (16), and human AQP9 (17, 18). With pK_a values of 3.9 for L-lactate, 4.4 for β-hydroxybutyrate, and 4.8 for acetate (see Table 1), protonation depends strongly on the prevalent pH (13). The nature of the species conducted by the AQP, anion *versus* neutral acid, and the underlying mechanism, however, are unclear.

AQP9, as a member of the mammalian aquaglyceroporins that also include AQP3 (19), AQP7 (20), and AQP10 (21), stands out by its apparent conductance for a large variety of substrates. In addition to glycerol, AQP9 was found to be permeable to carbamides, purines, pyrimidines, ketone bodies, and monocarboxylates (17). Nevertheless, the protein sequence of AQP9 appears inconspicuous with respect to the NPA motifs and ar/R selectivity filter (2). A 7 Å resolution projection structure from 2D crystals (22), however, indicates that the AQP9 pore is slightly wider than that of the prototypical GlpF from *Escherichia coli* (9).

AQP9 is expressed in hepatic cells (23) where it channels glycerol in for gluconeogenesis (24, 25) and urea out to release metabolic nitrogen waste (26). The distribution of AQP9 in the

This work was supported by Deutsche Forschungsgemeinschaft Grant Be2253/7-1. The authors declare that they have no conflicts of interest with the contents of this article. The content is solely the responsibility of the authors and does not necessarily represent the official views of the National Institutes of Health.

This article contains supplemental Fig. S1.

[1] Present address: Dept. of Biochemistry and Molecular Biology, University of Hamburg, 20148 Hamburg, Germany.

[2] To whom correspondence should be addressed: Dept. of Pharmaceutical and Medicinal Chemistry, Christian-Albrechts-University of Kiel, Gutenbergstr. 76, 24118 Kiel, Germany. Tel.: 49-431-880-1809; Fax: 49-431-880-1352; E-mail: ebeitz@pharmazie.uni-kiel.de.

[3] The abbreviations used are: AQP, aquaporin; NPA, Asn-Pro-Ala region; ar/R, aromatic/arginine constriction; GlpF, glycerol facilitator; FNT, formate-nitrite transporter; DNP, 2,4-dinitrophenol.

brain, in particular at the blood-brain barrier, in glia cells, and in catecholaminergic neurons, suggests physiological functions in energy provision in the form of ketone bodies, and in the protection of neurons in pathological ischemia by channeling L-lactate (27, 28).

Here, we show that the positive surface electrostatics of AQP9 is crucial for attracting monoacid anions, protonation of the substrate, and passage of the neutral species. We further found that protonation efficiency increased with substrate size compensating impediments to mobility of the larger molecules. As a consequence, at neutral pH, all tested monoacid substrates, *i.e.* acetic acid, L-lactic acid, and particularly β-hydroxybutyric acid, passed AQP9 at rates that suggest physiological relevance.

Results

Permeability of AQP9 for lactate/lactic acid increases with lower pH

Initially, we determined the pH profiles of lactate/lactic acid permeability of the human aquaglyceroporin AQP9 and murine AQP7, for which monoacid permeability has not been described before. We expressed AQP9 and AQP7 in yeast, prepared osmosensitive protoplasts, and subjected them to a 50 mM inwardly directed gradient of lactate/lactic acid in the range of pH 3–7. Cellular volume changes were monitored via changes in the light scattering intensity (Fig. 1*A*) (29). In a first, rapid phase (<15 s), osmotic water efflux via the expressed AQP and across the plasma membrane decreases the cell volume as indicated by an increase in light scattering. In a second, slower phase (>15 s), volume will be regained because of solute influx and a secondary osmotic inflow of water resulting in a decrease in the light scattering intensity. Lactate/lactic acid permeability of AQP9-expressing yeast cells increased toward lower pH (Fig. 1*A*, *left panel*), whereas with AQP7 hardly any permeability was detectable at all pH conditions (Fig. 1*B*, *left panel*). To test for pH effects on the AQP protein integrity and to relate the lactate/lactic acid permeability of AQP9 and AQP7 to a common, similarly sized and neutral substrate, we determined glycerol permeability. Glycerol has a molar mass of 92 g mol^{-1}, and lactic acid has a molar mass of 90 g mol^{-1} at a similar van der Waals volume (88.0 *versus* 81.6 $Å^3$; Table 1). However, with a pK_a of 14.2, glycerol will remain neutral in aqueous solution independent of the pH. AQP9 was functional at all tested pH conditions, and glycerol permeability decreased by 45% with increasing buffer acidity (Fig. 1*A*, *right panel*). AQP7 was highly permeable for glycerol at a pH of 5 and greater but exhibited a sudden loss of functionality at pH 4 and below (Fig. 1*B*, *right panel*). This pH dependence of AQP7 has not been shown before and is probably due to protonation of critical aspartate (pK_a = 3.9) and/or glutamate residues (pK_a = 4.3). From the light scattering traces, we extracted the permeability coefficients (P_{sol}) by exponential fittings of the second, solute diffusion phase (6). We plotted the permeability coefficients against the pH and obtained sigmoidal curves for lactate/lactic acid permeability of AQP9, whereas the curve for AQP7 was flat (Fig. 1*C*, *left panel*). The lactate/lactic acid permeability rates for AQP9 were maximal at the most acidic assay condition,

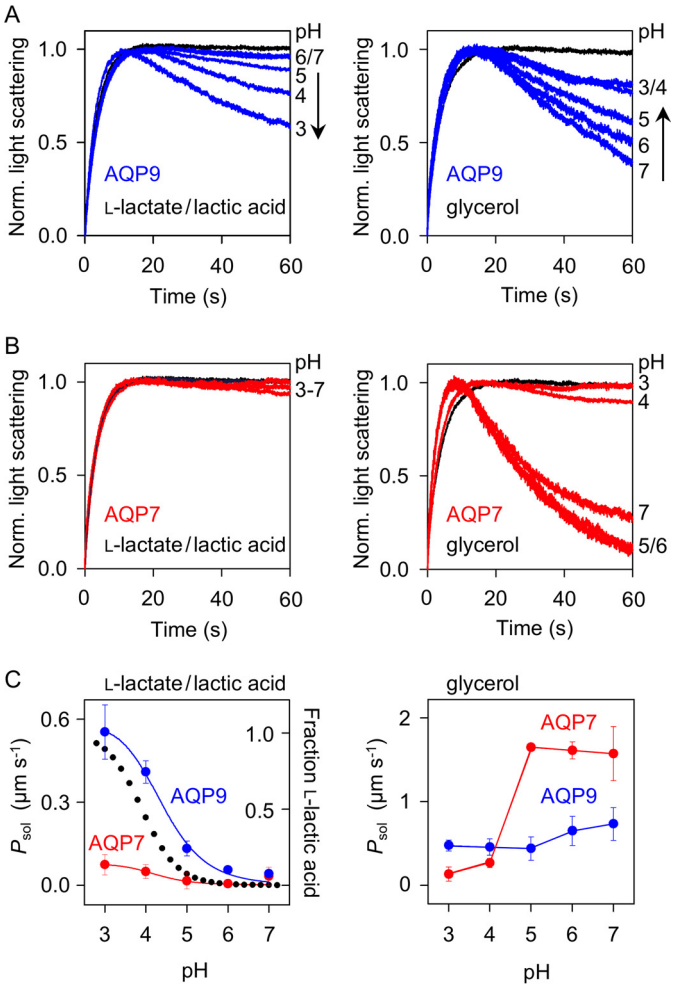

Figure 1. Light scattering assays of pH-dependent L-lactic acid and glycerol permeability. The initial, rapid increase in light scattering is due to osmotic water efflux from the yeast protoplasts in a 50 mM solute gradient. The subsequent, slower decrease in light scattering derives from influx of the solute and a concomitant osmotic water flow. *A*, human AQP9 (*blue*) exhibits increasing L-lactate/lactic acid (*left panel*) and decreasing glycerol permeability (*right panel*) toward acidic assay conditions. The *black trace* shows the behavior of non-expressing cells. *B*, murine AQP7 (*red*) shows minimal L-lactate/lactic acid similar to non-expressing cells (*black*). Glycerol permeability ceases abruptly between pH 4 and 5. *C*, permeability coefficients, P_{sol}, derived from exponential fittings of the solute uptake phases were plotted against the pH. Note the different scales of the *ordinates*. The *dotted line* indicates the fraction of protonated, neutral L-lactic acid of the total lactate according to the Henderson-Hasselbalch equation. All experiments were done in triplicate; the *error bars* denote S.E.

pH 3. Here, the fraction of neutral lactic acid is 0.9 of the total lactate, and the observed permeability coefficient (0.55 ± 0.10 μm s^{-1}) matched that of glycerol (0.48 ± 0.06 μm s^{-1}; Fig. 1*C*, *right panel*). A plot depicting the permeability ratio for lactate/glycerol as a function of pH is shown in supplemental Fig. S1. The pH profile suggests passage of the neutral, protonated lactic acid form via AQP9. If the charged lactate anion was the permeating species, a reversed sigmoidal curve would have resulted with decreasing rates toward lower pH. Quite unexpectedly, comparison of the permeability rates with the fraction of available neutral lactic acid at each tested pH (Fig. 1*C*, *dotted line*) revealed a shift by 0.6 log units, *i.e.* the substrate permeability is $10^{0.6}$ (four) times higher than predicted. Because of full blockage of AQP7 at pH 3 and small residual functionality of

Table 1
AQP9 substrate properties and permeability in the physiological pH range

Substrate	pK_a	Molecular mass	van der Waals volume	Observed Δ pK_a	Integral of P_{sol}, pH 5.5–7
		Da	*Å*^{3}		$\mu m\ s^{-1}$
Glycerol	14.2	92	88.0		0.991
Acetic acid	4.8	60	55.9	0	0.425
L-Lactic acid	3.9	90	81.6	0.6	0.053
β-Hydroxybutyric acid	4.4	104	98.5	1.0	0.120

14% at pH 4 (Fig. 1*C*, *right panel*), the data for AQP7 could be analyzed only at pH 5, 6, and 7. In this range, AQP7 exhibited 2–4-fold higher glycerol permeability than AQP9 (Fig. 1*C*, *right panel*). However, permeability for lactic acid was at best one-eighth that of AQP9 (Fig. 1*C*, *left panel*, and ratio plot in supplemental Fig. S1). This and the offset between the existing lactic acid fraction in the buffer and the observed permeability rates clearly hint at a specially adapted mechanism of AQP9 to facilitate lactate/lactic acid permeability.

AQP9 channels neutral lactic acid independent of the transmembrane proton gradient

The protonation state of the AQP9-passing substrate species directly affects the proton concentration in the buffer. Passage of the neutral, protonated lactic acid species via AQP9 would lead to alkalization of the media caused by a loss of protons, whereas uptake of the lactate anion would lead to acidification (30). Hence, we monitored pH changes in the weakly buffered external solution using a pH electrode during lactate/lactic acid uptake (Fig. 2*A*). AQP9-expressing yeast cells steadily alkalized the buffer confirming uptake of the protonated lactic acid substrate, whereas non-expressing cells marginally alkalized the buffer.

We next addressed the question whether AQP9 has adopted secondary transporter-like functions by making use of a transmembrane proton gradient. Therefore, we measured lactic acid influx via AQP9 at an external of pH 4, *i.e.* a 1000:1 inward proton gradient (assuming a cytosolic pH of 7), with and without addition of a protonophore, 2,4-dinitrophenol (DNP) (31). Despite disruption of the proton gradient by DNP, the lactic acid permeability of AQP9 remained unaltered (Fig. 2*B*). The data indicate that AQP9 acts as a channel, and permeability rates are determined solely by the availability and transmembrane gradient of neutral lactic acid.

The extracellular protein surface of AQP9 is positively charged

Our observation that AQP9 conducts lactic acid at a four times higher rate than predicted from the pH-dependent availability of lactic acid, whereas AQP7 exhibited very low lactic acid permeability only at the most extreme acidic pH remained puzzling. We hypothesized that the degree of electrostatic attraction of negatively charged substrate molecules may be different between AQP9 and AQP7 leading to a higher local concentration of lactate/lactic acid at the AQP9 protein surface. Calculation of the Poisson-Boltzmann electrostatics (32) showed a strongly positive extracellular surface of an AQP9 structure model (33), whereas AQP7 was oppositely charged (Fig. 3). To connect the surface properties to specific amino acid positions, we scanned the AQP9 sequence for cationic residues with a particular focus on sites where other AQPs carry non-charged residues (34). This way, we identified three candidate residues (Fig. 3*A*, *top center*): His^{146} located just above the ar/R constriction site and two arginines, Arg^{51} and Arg^{53}, in the extracellular loop A connecting transmembrane spans 1 and 2 (Fig. 3*B*). The latter form a central elevation at the extracellular face of the AQP9 tetramer. To evaluate effects of the candidate residues, we calculated the surface charge of the respective AQP9-H146A, AQP9-R51A,R53A, and AQP9-R51E,R53E mutants (Fig. 3*A*, *bottom panels*). Although AQP9-H146A showed a small reduction in positive surface electrostatics, AQP9-R51A,R53A appeared fairly neutral, and AQP9-R51E,E53E exhibited a strongly negative protein surface similar in extent to AQP7 (Fig. 3*A*).

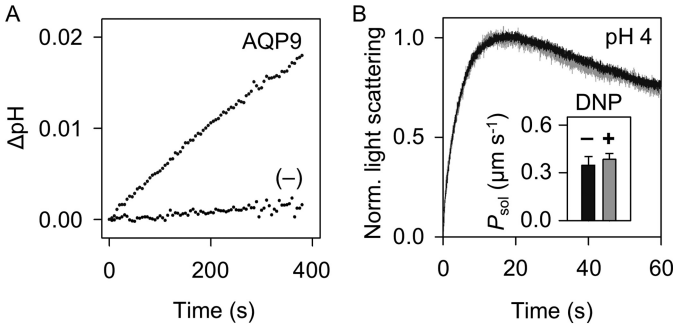

Figure 2. Alkalization of the external solution during L-lactate/lactic acid uptake and independency from the transmembrane gradient. *A*, the changes in pH of the weakly buffered external solution (pH 5) were monitored using a pH electrode in the presence of yeast cells with or without AQP9 expression. *B*, proton decoupling by DNP does not affect L-lactate/lactic acid uptake in a 1000:1 inward substrate gradient. *Error bars* indicate the S.E. from three independent experiments. *Norm.*, normalized.

AQP9 surface electrostatics determines lactic acid permeability

We generated the AQP9 mutants AQP9-H146A, AQP9-R51A,R53A, and AQP9-R51E,E53E for functional assays in yeast. Western blot analysis confirmed expression of the AQP9 mutants at equal or somewhat greater levels than wild-type AQP9 (Fig. 4*A*). Next, we assayed for glycerol permeability at neutral pH to evaluate general protein functionality (Fig. 4*B*). Here, quite unexpectedly, AQP9-R51A,R53A came with a loss of function and had to be eliminated from the test set. AQP9-H146A and AQP9-R51E,E53E conducted glycerol at equal rates as wild-type AQP9 and, hence, were usable for lactic acid permeability assays. AQP9-H146A showed a pH profile of lactic acid permeability (Fig. 4*C*) identical to that of wild-type AQP9 (Fig. 4*C*, *dashed line*). In the AQP9-R51E,E53E mutant, however, lactate permeability turned out to be strongly reduced across the pH 3–7 range (Fig. 4*D* and supplemental Fig. S1); however, glycerol permeability was

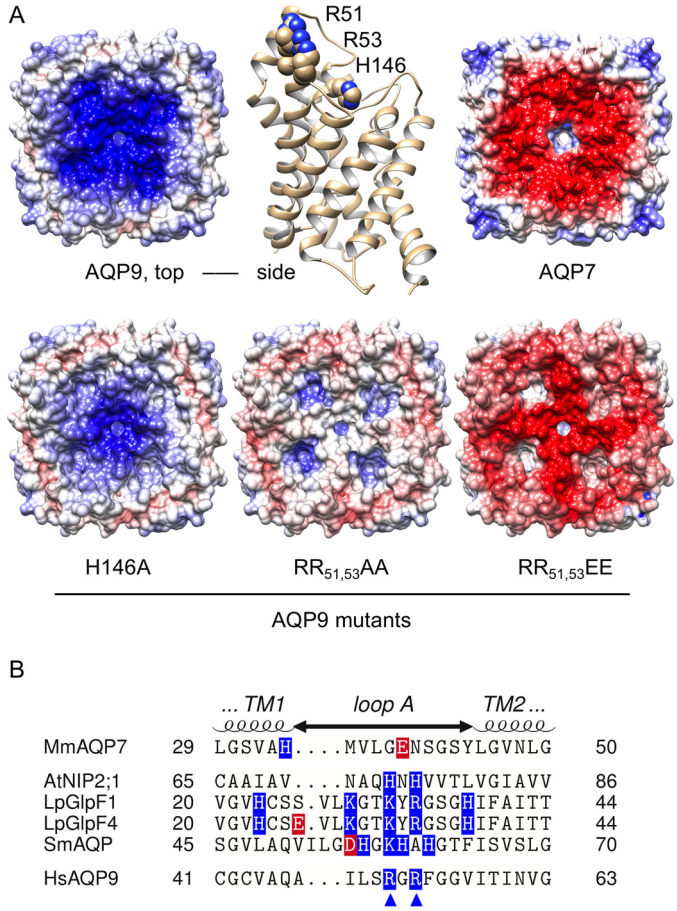

Figure 3. AQP surface charge. *A*, Poisson-Boltzmann surface electrostatics of tetrameric wild-type and mutant human AQP9 and murine AQP7. The side-view cartoon of a AQP9 protomer (*top center panel*) depicts the position of the surface arginines (Arg^{51} and Arg^{53}) and histidine (His^{146}). *B*, section of a protein alignment of murine AQP7 (*Mus musculus*), human AQP9 (*Homo sapiens*), and L-lactic acid conducting AQPs: *A. thaliana* NIP2;1, *L. plantarum* GlpF1 and 4, and *S. mansoni* AQP. Shown is the extracellular loop A between transmembrane spans 1 and 2. Charged residues are highlighted in *red* (acidic) and *blue* (basic). The AQP9 Arg^{51}/Arg^{53} positions are labeled by *triangles*. The alignment was set using TEXshade (34).

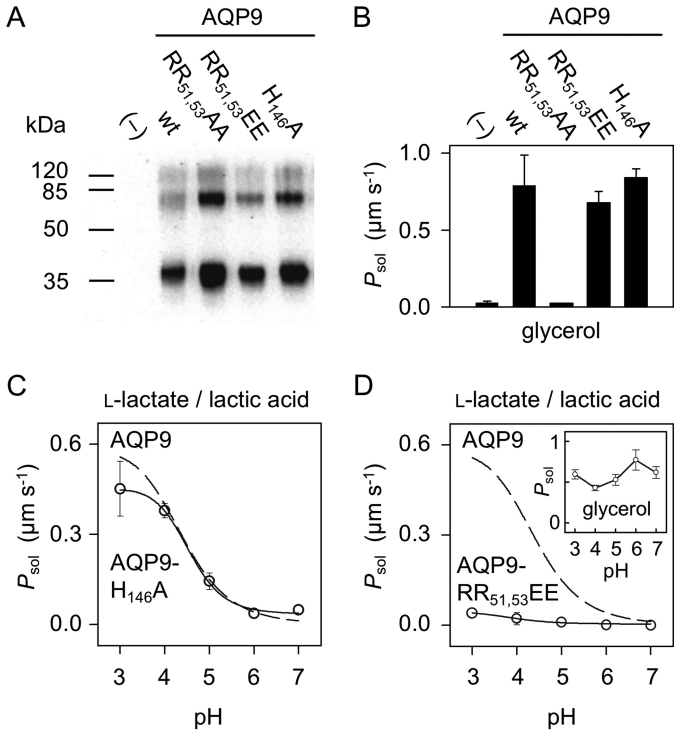

Figure 4. Expression and permeability of AQP9 mutants with altered surface electrostatics. *A*, Western blot (75 μg of total protein/lane) showing expression of AQP wild-type and mutants as detected via an engineered N-terminal hemagglutinin epitope tag (total of 39 kDa). The additional bands at 78 kDa and below and above 120 kDa correspond to the partially SDS-resistant AQP di-, tri-, and tetramers. *B*, glycerol permeability determined at pH 7 by light scattering. *C* and *D*, pH profiles of L-lactate/lactic acid permeability via AQP9-H_{146}A (*C*) and AQP9-R51E,E53E (*D*). The *inset* in *D* shows pH-independent glycerol permeability of AQP9-R51E,E53E. For comparison, the position of the curve of wild-type AQP9 is shown by the *dashed line*. The *error bars* denote S.E. from three independent experiments.

observed and equal to wild-type AQP9 at all pH conditions, indicating protein functionality (Fig. 4*D*, *inset*). The very-low lactic-acid conductance in combination with high glycerol permeability mirrors the properties of AQP7 (Fig. 4*D*) and may be directly attributable to repulsion of lactate anions by the negative surface electrostatics.

Acetic and β-hydroxybutyric acid show shifted permeability profiles

To test for an influence of substrate pK_a and size, we determined the pH profiles of AQP9 conductance for acetate/acetic acid (pK_a = 4.8; van der Waals volume 55.9 Å^3) and β-hydroxybutyrate/β-hydroxybutyric acid (pK_a = 4.4; 98.5 Å^3; Table 1). As with lactic acid, permeability for both physiological substrates increased toward lower pH, indicating passage of the neutral acids via AQP9 (Fig. 5). However, correlation of the permeability rates to the available fractions of neutral, protonated substrate acid in the buffer (Fig. 5, *dotted lines*) uncovered major differences: Permeability of acetic acid directly corresponded to the available neutral acid fraction, whereas with

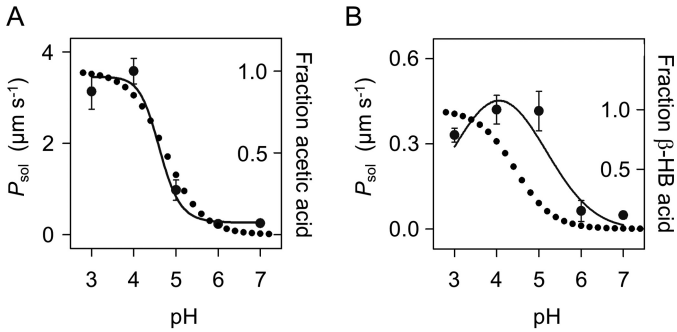

Figure 5. AQP9 pH profiles for acetic (*A*) and β-hydroxybutyric acid permeability (*B*). The pH-dependent fractions of protonated, neutral acetic and β-hydroxybutyric acid (β-*HB*) are indicated by the *dotted lines*. Note the different scales of the *ordinates*. All experiments were done in triplicate; the *error bars* denote S.E.

β-hydroxybutyric acid, availability and permeability curves were shifted by a full log unit, *i.e.* β-hydroxybutyric acid passed AQP9 10 times better than predicted from the free substrate concentration.

Discussion

Our results indicate that the protein surface charge of AQPs plays a critical role in the attraction and repulsion of weak monoacids. The negatively charged protein surfaces of murine

AQP7 and AQP9-R51E,E53E effectively prevent lactate/lactic acid from approaching the pore, resulting in low permeability. This negative electrostatic shield at the surface (repelling anions) combined with the positive field generated by the NPA and ar/R constrictions (excluding cations) can be seen as a so-far undescribed, double-layered selection mechanism of AQPs against charged molecules. It is discussed, however, that a negative protein surface attracts ammonium cations, NH_4^+, as a feature of AQPs that conduct ammonia, NH_3 (35). In turn, a positively charged protein surface, as shown in this study on human AQP9, increases the local acid anion concentration promoting protonation and passage of the neutralized monoacid species via the AQP.

The extent of an electrostatic field is defined by the charge and the dielectric properties of the environment (36, 37). In a physiological setting with water as the universal solvent, *i.e.* a high dielectric constant, ϵ, of 78, the outreach of the field is small. Therefore, to act on a long range, the attracting protein surface must be highly charged. In AQP9, this is accomplished by eight arginine residues that are concentrated at the central interface of the AQP tetramer. By sequence comparison we found that other AQPs with reported lactic acid permeability carry positive residues at the respective positions, whereas in murine AQP7 a glutamate results in negative electrostatics (Fig. 3*B*). To date, there are few examples of AQPs with apparent monoacid conductance. This may be because the structural requirements are rarely met in the AQP family. Therefore, the sporadic cases of positive charge accumulation in the center of the tetramer surface is likely to be physiologically meaningful, *e.g.* for lactic acid permeability of the *Lactobacillus* GlpFs (16), or lactic and β-hydroxybutyric acid permeability of AQP9 in the human brain (17, 27, 28). In fact, in the physiological pH range of 5.5–7, AQP9 permeability of L-lactic acid was 5%, and that of β-hydroxybutyric acid was even 12% that of glycerol (see integral of P_{sol} over the physiological pH interval; Table 1).

Among the monoacid substrates, L-lactic and β-hydroxybutyric acid showed one-eighth and somewhat more than one-quarter, respectively, of the acetic acid permeability via AQP9 in the physiological pH range (Table 1). This is quite surprising because lactic acid is 10 times more acidic, which decreases the fraction of available neutral substrate by the same factor, and 46% larger than acetic acid, which should further impede passage through the channel. The acidity of β-hydroxybutyric acid is intermediate, yet its molecular volume is even greater by 76%. Key to this counterintuitive phenomenon seems to be a size-dependent disparity between substrate acidity in the aqueous bulk solution and in proximity to the protein surface, illustrated by the offset between the calculated neutral substrate fraction and measured permeability curves in Figs. 1*C* and 5 (compare Van der Waals volume and observed ΔpK_a in Table 1). We noted a similar behavior when studying the structurally related formate-nitrite transporter family (FNT) (38). We found that as part of the transport mechanism, a substrate anion, *e.g.* formate, is attracted by a positively charged lysine and funneled into a hydrophobic vestibule, *i.e.* a low-ϵ dielectric environment (30, 31). The resulting reduction of substrate acidity initiates protonation by the bulk solution and transport of the neutral substrate via lipophilic constriction sites. The apparent acidity decreased with increasing substrate size, which we explained by better shielding from the bulk solution. Depending on the substrate, we observed a pK_a shift of up to 3 units, *i.e.* the probability of transport at a given buffer pH was increased by 3 orders of magnitude. The situation in AQP9 is quite similar, though on a smaller scale: here, the arginines at positions 51 and 53 guide substrate anions into the channel vestibules of the individual AQP protomers yielding a ΔpK_a up to 1 unit, translating into an increase in permeability by 1 order of magnitude. Together, the FNT family and monoacid-conducting AQPs apparently employ a common mechanism of anion attraction and facilitation of protonation for passage of the neutral substrate species.

In addition to FNTs and AQPs, also other classes of proteins attract small molecule substrates or ligands via surface electrostatics. The best-studied example is probably the acetycholinesterase enzyme (39). Here, six negatively charged surface residues attract and guide the positively charged acetylcholine substrate into the catalytic center. A mutant enzyme with all six amino acids replaced with neutral residues, yet with the catalytic center unchanged, exhibited a 13-fold reduced catalytic efficiency (k_{cat}/K_m) (39). Similarly, in the nicotinergic acetylcholine receptor, exchange of negatively charged residues near the ligand-binding site reduced affinity (40). However, the number of such studies is low, probably because a quantitative readout is required for evaluation. Aquaporin permeability assays provide an easy to obtain and quantitative measure, which may be further exploited to assess the influence of surface electrostatics on small molecule attraction.

Experimental procedures

Plasmid constructs, yeast culture, and Western blots

Human AQP9 (NCBI Gene ID 366) and mouse AQP7 (NCBI Gene ID 11832) were cloned via SpeI and XhoI into the pDR196 vector (29). Site-directed mutagenesis was carried out by PCR using the QuikChange protocol (Agilent). For the AQP9-H146A mutant, the forward primer was 5′-GAAAATGCAACAGCAGCTATTTTTGCAACATAC-3′. For the Arg^{51}–Arg^{53} double mutants the forward primers were 5′-CAAGCTATTCTCAGT*XXX*GGA*XXX*TTTGGAGGGGTCATC-3′, where *XXX* = GCT for R51A,R53A and *XXX* = GAA for R51E,R53E. DNA mutations were confirmed by sequencing. *Saccharomyces cerevisiae* strain W303-1A *jen1*Δ *ady2*Δ (MATa; leu2-3,112 trp1-1 can1-100 ura3-1 ade2-1 his3-11,15) lacking endogenous lactate transporters was kindly provided by M. Casal. The yeast cells were transformed with pDR196 plasmids encoding AQP9, AQP9-H146A, AQP9-R51A,R53A, AQP9-R51E,R53E, or AQP7 or with the empty plasmid using the lithium acetate/single stranded carrier DNA/polyethylenglycol procedure (41). Transformed yeast was grown at 29 °C in selective medium without uracil and containing adenine, histidine, leucine, tryptophan, and 2% (w/v) glucose. All plasmid constructs carry an N-terminal HA epitope tag and a C-terminal 10× His tag. The HA tag was used for detection by Western blotting using a monoclonal mouse anti-HA antibody (1:5000; Roche) and a horseradish peroxidase-conjugated secondary

antibody (1:2000; Jackson ImmunoResearch) for ECL detection (Amersham Biosciences).

Yeast protoplast preparation and stopped-flow light scattering assays

Cultured yeast cells were collected at an A_{600} of 1 in mid-logarithmical phase (2000 × *g* at 4 °C), washed, and incubated for 15 min in 2 ml MOPS buffer (50 mM, pH 7.2, 0.2% 2-mercaptoethanol). For protoplastation, per gram of wet yeast 4 ml of MOPS/2-mercaptoethanol buffer containing 1.8 M sucrose, 200 units of zymolyase-20 T (MP Biomedicals, Illskirch, France), and 100 mg of bovine serum albumin fraction V (Roth, Karlsruhe, Germany) were added. The cell suspension was agitated for 60 min at 29 °C by orbital shaking at 100 rpm. Protoplasts were collected (2000 × *g*, 4 °C), washed, and resuspended in 2 ml of buffer (pH 7: 20 mM MOPS; pH 6: MES; pH 3, 4, and 5: citric acid, containing 1.2 M sucrose, 50 mM NaCl, and 5 mM $CaCl_2$). The protoplast suspensions were diluted to an A_{600} of 2 before the assay. The measurements were done at 20 °C in a stopped-flow apparatus (SFM-300; BioLogic, Claix, France) with a dead time of ~5 ms, a total flow rate of 7 ml s^{-1}, and a total injection volume of 150 μl. Hypertonic permeability assays were carried out by rapidly mixing the protoplasts with the same volume of buffer (described above) supplemented with 100 mM solute (glycerol, acetate, L-lactate, β-D/L-hydroxybutyrate), generating a 50 mM inward gradient. For measuring the effect of protonophores at pH 4, 1 mM dinitrophenol was added 30 min prior to the assay. Protoplast volume changes were monitored by measuring the intensity of 90° light scattering at 546 nm. In each experiment 6–9 traces were averaged. The permeability coefficients (P_{sol}, μm s^{-1}) were obtained by exponential fitting (Biokine software) of the second phase of the light scattering curves using $P_{sol} = |dI/dt| \cdot (V_0 \cdot C_{out})/(S_0 \cdot C_{diff})$ (6), with dI/dt being the slope of the intensity curve, V_0 and S_0 are as above, C_{out} is the total external solute concentration (1.25 M for glycerol; 1.3 M for monocarboxylates), and C_{diff} is the chemical solute gradient (0.05 M). Three biological replicates were done for each experimental condition, and the S.E. was calculated.

Media alkalization measured by pH electrode

200-ml yeast cultures were grown overnight to an A_{600} of 1 and harvested (4000 × *g*, 5 min), washed, and resuspended in 2 ml of 4 mM citric acid buffer, pH 5, containing 0.5% 6-desoxyglucose. The cells were resuspended to an A_{600} of 60. 1 ml of cell suspension plus 7 ml of water were put on a magnetic stirrer, and pH changes were monitored with a glass membrane electrode after addition of 20 mM L-lactate. In each experiment, three pH curves were averaged, and the resulting time constants were determined by linear fitting using SigmaPlot. Three biological replicates were done.

Electrostatics calculations

AQP9 and AQP7 protein structure models were generated based on *E. coli* GlpF using SwissModel (33) and displayed with the Chimera software (42). Linear Poisson-Boltzmann electrostatics were calculated by calling the PDB2PQR (43, 44) and Adaptive Poisson-Boltzmann Solver (APBS) (32) algorithms from within Chimera.

Author contributions—M. R. conducted most of the experiments, analyzed the results, and wrote parts of the paper. D. R. started the project and carried out initial permeability measurements. E. B. conceived the idea for the project, ran the APBS electrostatics analyses, and wrote the paper with M. R.

Acknowledgments—We thank B. Henke and A. Fuchs for technical assistance, as well as M. Casal for providing the jen1Δ ady2Δ yeast strain. Molecular graphics and analyses were performed with the UCSF Chimera package. Chimera is developed by the Resource for Biocomputing, Visualization, and Informatics at the University of California, San Francisco (which is supported by NIGMS P41-GM103311).

References

1. Zardoya, R. (2005) Phylogeny and evolution of the major intrinsic protein family. *Biol. Cell* **97,** 397–414
2. Wu, B., and Beitz, E. (2007) Aquaporins with selectivity for unconventional permeants. *Cell. Mol. Life Sci.* **64,** 2413–2421
3. Murata, K., Mitsuoka, K., Hirai, T., Walz, T., Agre, P., Heymann, J. B., Engel, A., and Fujiyoshi, Y. (2000) Structural determinants of water permeation through aquaporin-1. *Nature* **407,** 599–605
4. Beitz, E., Wu, B., Holm, L. M., Schultz, J. E., and Zeuthen, T. (2006) Point mutations in the aromatic/arginine region in aquaporin 1 allow passage of urea, glycerol, ammonia and protons. *Proc. Natl. Acad. Sci. U.S.A.* **103,** 269–274
5. Wu, B., Steinbronn, C., Alsterfjord, M., Zeuthen, T., and Beitz, E. (2009) Concerted action of two cation filters in the aquaporin water channel. *EMBO J.* **28,** 2188–2194
6. Wree, D., Wu, B., Zeuthen, T., and Beitz, E. (2011) Requirement for asparagine in the aquaporin NPA sequence signature motifs for cation exclusion. *FEBS J.* **278,** 740–748
7. Li, H., Chen, H., Steinbronn, C., Wu, B., Beitz, E., Zeuthen, T., and Voth, G. A. (2011) Enhancement of proton conductance by mutations of the selectivity filter of aquaporin-1. *J. Mol. Biol.* **407,** 607–620
8. Kosinska Eriksson, U., Fischer, G., Friemann, R., Enkavi, G., Tajkhorshid, E., and Neutze, R. (2013) Subangstrom resolution X-ray structure details aquaporin-water interactions. *Science* **340,** 1346–1349
9. Fu, D., Libson, A., Miercke, L. J., Weitzman, C., Nollert, P., Krucinski, J., and Stroud, R. M. (2000) Structure of a glycerol-conducting channel and the basis for its selectivity. *Science* **290,** 481–486
10. Yasui, M., Hazama, A., Kwon, T. H., Nielsen, S., Guggino, W. B., and Agre, P. (1999) Rapid gating and anion permeability of an intracellular aquaporin. *Nature* **402,** 184–187
11. Ikeda, M., Beitz, E., Kozono, D., Guggino, W. B., Agre, P., and Yasui, M. (2002) Characterization of aquaporin-6 as a nitrate channel in mammalian cells. Requirement of pore-lining residue threonine 63. *J. Biol. Chem.* **277,** 39873–39879
12. Liu, K., Kozono, D., Kato, Y., Agre, P., Hazama, A., and Yasui, M. (2005) Conversion of aquaporin 6 from an anion channel to a water-selective channel by a single amino acid substitution. *Proc. Natl. Acad. Sci. U.S.A.* **102,** 2192–2197
13. Rambow, J., Wu, B., Rönfeldt, D., and Beitz, E. (2014) Aquaporins with anion/monocarboxylate permeability: mechanisms, relevance for pathogen-host interactions. *Front. Pharmacol.* **5,** 199
14. Choi, W.-G., and Roberts, D. M. (2007) *Arabidopsis* NIP2;1, a major intrinsic protein transporter of lactic acid induced by anoxic stress. *J. Biol. Chem.* **282,** 24209–24218
15. Faghiri, Z., Camargo, S. M., Huggel, K., Forster, I. C., Ndegwa, D., Verrey, F., and Skelly, P. J. (2010) The tegument of the human parasitic worm *Schistosoma mansoni* as an excretory organ: the surface aquaporin SmAQP is a lactate transporter. *PLoS One* **5,** e10451

16. Bienert, G. P., Desguin, B., Chaumont, F., and Hols, P. (2013) Channel-mediated lactic acid transport: a novel function for aquaglyceroporins in bacteria. *Biochem. J.* **454,** 559–570
17. Tsukaguchi, H., Shayakul, C., Berger, U. V., Mackenzie, B., Devidas, S., Guggino, W. B., van Hoek, A. N., and Hediger, M. A. (1998) Molecular characterization of a broad selectivity neutral solute channel. *J. Biol. Chem.* **273,** 24737–24743
18. Tsukaguchi, H., Weremowicz, S., Morton, C. C., and Hediger, M. A. (1999) Functional and molecular characterization of the human neutral solute channel aquaporin-9. *Am. J. Physiol.* **277,** F685–F696
19. Ishibashi, K., Sasaki, S., Fushimi, K., Uchida, S., Kuwahara, M., Saito, H., Furukawa, T., Nakajima, K., Yamaguchi, Y., and Gojobori, T. (1994) Molecular cloning and expression of a member of the aquaporin family with permeability to glycerol and urea in addition to water expressed at the basolateral membrane of kidney collecting duct cells. *Proc. Natl. Acad. Sci. U.S.A.* **91,** 6269–6273
20. Ishibashi, K., Kuwahara, M., Gu, Y., Kageyama, Y., Tohsaka, A., Suzuki, F., Marumo, F., and Sasaki, S. (1997) Cloning and functional expression of a new water channel abundantly expressed in the testis permeable to water, glycerol, and urea. *J. Biol. Chem.* **272,** 20782–20786
21. Ishibashi, K., Morinaga, T., Kuwahara, M., Sasaki, S., and Imai, M. (2002) Cloning and identification of a new member of water channel (AQP10) as an aquaglyceroporin. *Biochim. Biophys. Acta* **1576,** 335–340
22. Viadiu, H., Gonen, T., and Walz, T. (2007) Projection map of aquaporin-9 at 7 Å resolution. *J. Mol. Biol.* **367,** 80–88
23. Elkjaer, M., Vajda, Z., Nejsum, L. N., Kwon, T., Jensen, U. B., Amiry-Moghaddam, M., Frøkiaer, J., and Nielsen, S. (2000) Immunolocalization of AQP9 in liver, epididymis, testis, spleen, and brain. *Biochem. Biophys. Res. Commun.* **276,** 1118–1128
24. Calamita, G., Gena, P., Ferri, D., Rosito, A., Rojek, A., Nielsen, S., Marinelli, R. A., Frühbeck, G., and Svelto, M. (2012) Biophysical assessment of aquaporin-9 as principal facilitative pathway in mouse liver import of glucogenetic glycerol. *Biol. Cell* **104,** 342–351
25. Gena, P., Mastrodonato, M., Portincasa, P., Fanelli, E., Mentino, D., Rodríguez, A., Marinelli, R. A., Brenner, C., Frühbeck, G., Svelto, M., and Calamita, G. (2013) Liver glycerol permeability and aquaporin-9 are dysregulated in a murine model of non-alcoholic fatty liver disease. *PLoS One* **8,** e78139
26. Jelen, S., Gena, P., Lebeck, J., Rojek, A., Praetorius, J., Frøkiaer, J., Fenton, R. A., Nielsen, S., Calamita, G., and Rützler, M. (2012) Aquaporin-9 and urea transporter-A gene deletions affect urea transmembrane passage in murine hepatocytes. *Am. J. Physiol. Gastrointest. Liver Physiol.* **303,** G1279–G1287
27. Badaut, J., Petit, J.-M., Brunet, J.-F., Magistretti, P. J., Charriaut-Marlangue, C., and Regli, L. (2004) Distribution of Aquaporin 9 in the adult rat brain: preferential expression in catecholaminergic neurons and in glial cells. *Neuroscience* **128,** 27–38
28. Badaut, J., and Regli, L. (2004) Distribution and possible roles of aquaporin 9 in the brain. *Neuroscience* **129,** 971–981
29. Song, J., Almasalmeh, A., Krenc, D., and Beitz, E. (2012) Molar concentrations of sorbitol and polyethylene glycol inhibit the *Plasmodium* aquaglyceroporin but not that of *E. coli*: involvement of the channel vestibules. *Biochim. Biophys. Acta* **1818,** 1218–1224
30. Wiechert, M., and Beitz, E. (2017) Mechanism of formate-nitrite transporters by dielectric shift of substrate acidity. *EMBO J.* **36,** 949–958
31. Wu, B., Rambow, J., Bock, S., Holm-Bertelsen, J., Wiechert, M., Soares, A. B., Spielmann, T., and Beitz, E. (2015) Identity of a *Plasmodium* lactate/H^+ symporter structurally unrelated to human transporters. *Nat. Commun.* **6,** 6284
32. Czodrowski, P., Dramburg, I., Sotriffer, C. A., and Klebe, G. (2006) Development, validation, and application of adapted PEOE charges to estimate pK_a values of functional groups in protein-ligand complexes. *Proteins* **65,** 424–437
33. Biasini, M., Bienert, S., Waterhouse, A., Arnold, K., Studer, G., Schmidt, T., Kiefer, F., Gallo Cassarino, T., Bertoni, M., Bordoli, L., and Schwede, T. (2014) SWISS-MODEL: modelling protein tertiary and quaternary structure using evolutionary information. *Nucleic Acids Res.* **42,** W252–W258
34. Beitz, E. (2000) TEXshade: shading and labeling of multiple sequence alignments using LaTeX2e. *Bioinformatics* **16,** 135–139
35. Kirscht, A., Kaptan, S. S., Bienert, G. P., Chaumont, F., Nissen, P., de Groot, B. L., Kjellbom, P., Gourdon, P., and Johanson, U. (2016) Crystal structure of an ammonia-permeable aquaporin. *PLoS Biol.* **14,** e1002411
36. Náray-Szabó, G. (1989) Electrostatic complementarity in molecular associations. *J. Mol. Graph.* **7,** 76–81, 98
37. Batra, J., Szabó, A., Caulfield, T. R., Soares, A. S., Sahin-Tóth, M., and Radisky, E. S. (2013) Long-range electrostatic complementarity governs substrate recognition by human chymotrypsin C, a key regulator of digestive enzyme activation. *J. Biol. Chem.* **288,** 9848–9859
38. Wang, Y., Huang, Y., Wang, J., Cheng, C., Huang, W., Lu, P., Xu, Y. N., Wang, P., Yan, N., and Shi, Y. (2009) Structure of the formate transporter FocA reveals a pentameric aquaporin-like channel. *Nature* **462,** 467–472
39. Radić, Z., Kirchhoff, P. D., Quinn, D. M., McCammon, J. A., and Taylor, P. (1997) Electrostatic influence on the kinetics of ligand binding to acetylcholinesterase: distinctions between active center ligands and fasciculin. *J. Biol. Chem.* **272,** 23265–23277
40. Osaka, H., Sugiyama, N., and Taylor, P. (1998) Distinctions in agonist and antagonist specificity conferred by anionic residues of the nicotinic acetylcholine receptor. *J. Biol. Chem.* **273,** 12758–12765
41. Gietz, R. D., Schiestl, R. H., Willems, A. R., and Woods, R. A. (1995) Studies on the transformation of intact yeast cells by the LiAc/SS-DNA/PEG procedure. *Yeast* **11,** 355–360
42. Pettersen, E. F., Goddard, T. D., Huang, C. C., Couch, G. S., Greenblatt, D. M., Meng, E. C., and Ferrin, T. E. (2004) UCSF Chimera: a visualization system for exploratory research and analysis. *J. Comput. Chem.* **25,** 1605–1612
43. Dolinsky, T. J., Czodrowski, P., Li, H., Nielsen, J. E., Jensen, J. H., Klebe, G., and Baker, N. A. (2007) PDB2PQR: expanding and upgrading automated preparation of biomolecular structures for molecular simulations. *Nucleic Acids Res.* **35,** W522–W525
44. Dolinsky, T. J., Nielsen, J. E., McCammon, J. A., and Baker, N. A. (2004) PDB2PQR: an automated pipeline for the setup, execution, and analysis of Poisson-Boltzmann electrostatics calculations. *Nucleic Acids Res.* **32,** W665–W667